SSC LABORATORY LIBRARY
JUN 2 9 1992

GEM TN-92-111

E_t Fluctuations in Pileup Events as a Function of Pseudorapidity

Eric G. Stern
University of Pittsburgh

June 9, 1992

Abstract:

The fluctuations in energy or transverse energy deposits in an ionization calorimeter determine the noise due to event pileup. For a calorimeter with uniform $\Delta\eta \times \Delta\phi$ segmentation, the fluctuations vary will vary with pseudorapidity ($\eta = -\log \tan \theta/2$) due to the interaction of the shower size with the changing physical size of the cell and particle particle density. We simulate the deposition of particles in a calorimeter using fairly simple assumptions about particle production distributions and energy deposition to determine the mean and fluctuations of the transverse energy measured in the simplified calorimeter. An analytic calculation of the same phenomenon agrees well with the simulation and provides an understanding of the contributing effects.

E_t fluctuations in pileup events as a function of pseudorapidity

Eric G. Stern

Department of Physics and Astronomy
University of Pittsburgh
Pittsburgh, PA 15260

ABSTRACT

The fluctuations in energy or transverse energy deposits in an ionization calorimeter determine the noise due to event pileup.[1] For a calorimeter with uniform $\Delta\eta \times \Delta\phi$ segmentation, the fluctuations vary will vary with pseudorapidity ($\eta = -\log\tan\frac{\theta}{2}$) due to the interaction of the shower size with the changing physical size of the cell and particle particle density. We simulate the deposition of particles in a calorimeter using fairly simple assumptions about particle production distributions and energy deposition to determine the mean and fluctuations of the transverse energy measured in the simplified calorimeter. An analytic calculation of the same phenomenom agrees well with the simulation and provides an understanding of the contributing effects.

Pileup noise in liquid ionization calorimeters operating at the SSC occurs because the data collection time for an event is longer than the interval between events. In real terms, at the SSC with a luminosity of $10^{33}\,\mathrm{cm}^{-2}\mathrm{sec}^{-1}$, an average of 1.6 minimum bias or low-p_t events occur every 16 ns. The response of a liquid argon calorimeter takes place over approximately 400 ns after a deposition. Depending on the occupancy of a calorimeter element, more than one energy deposition may be expected to contribute to the signal at any time. The fluctuations in the signal of a detecting element due to the background of constantly occuring minimum bias events can be shown to be[2]

$$\sigma_p^2 = I_{2p}\,\sigma_E^2 \tag{1}$$

where σ_p is the observed fluctuation in signal from a detector, I_{2p} is a constant depending only on signal processing parameters, and σ_E is the fluctuation in (transverse) energy deposit due to a single event. This relation applies as well to $E_t \equiv E\sin\theta$ which is the variable we will be considering. We now simulate the deposition of particles in a calorimeter to determine σ_E.

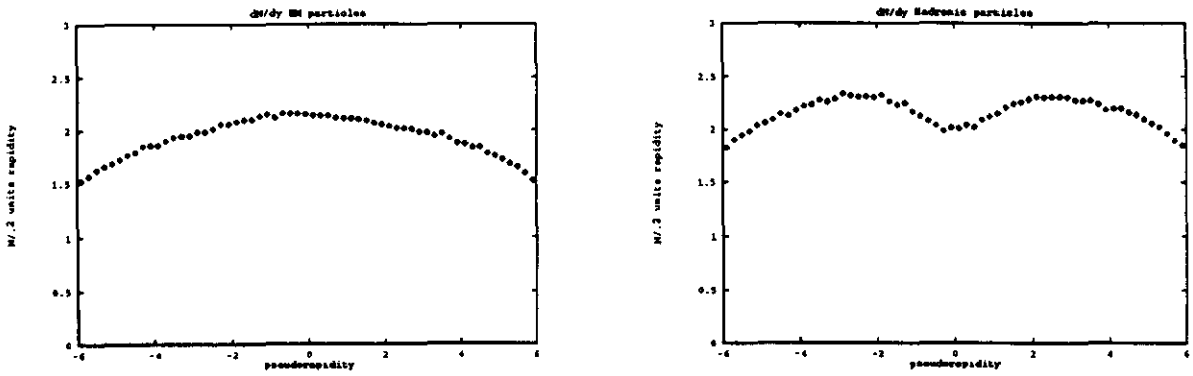

Figure 1.1: The particle density in $d\eta$ for electromagnetic and hadronic particles.

1. Simulation

We simulate a calorimeter with uniform segmentation of $\Delta\eta \times \Delta\phi = 0.04 \times 0.04$ up to maximum pseudorapidity of $\eta = 6$ exposed to hadronic collisions of the SSC. The calorimeter is 75 cm from the interaction point. Particles are assumed to produce a uniform circular shower on the face of the calorimeter. An electromagnetic shower has a radius of 2.2 cm while a hadronic shower has a radius of 14.0 cm.

The assumptions on particle production are motivated by the physics of hadron colliders and particle distributions from the ISAJET[3] event generation program. We used 10000 ISAJET generated two jet events between a p_t of 5 GeV and 10 GeV as a model of particle distributions for pileup events.

The number of particles per rapidity interval produced in hadronic collisions is largely independent of rapidity due to the Lorentz invariance of the fragmentation process. This is confirmed by ISAJET. Fig. 1.1 shows $dN/d\eta$, the number of particles produced in a unit rapidity interval as a function of η. The distributions are generally flat, with about a 20% variation. There are about 9 electromagnetic particles, and 11 hadronic particles produced per rapidity interval. The simulation uses these densities (9 and 11) to produce particles uniformly in η and ϕ over the coverage of the calorimeter.

The fragmentation process produces particles with a near-universal distribution of transverse energy which are then boosted to their final energy. In the ultra-relativistic regime, the final energy of the particle is $e_0 \cosh\eta$, where e_0 is the transverse energy characteristic of fragmentation. However, $\cosh\eta$ is $1/\sin\theta$, so the particle energy is inversely proportional to $\sin\theta$, and the transverse energy $E\sin\theta$ is roughly independent of η.

The mean transverse distributions for electromagnetic (e and γ particles), and for hadronic particles in the ISAJET generated two jet sample is shown in Fig. 1.2. ISAJET clearly produces particles that have a nearly uniformly constant transverse energy, about 0.2 GeV for electromagnetic particles, and 0.5 GeV for hadronic particles. The fluctuations in produced E_t are also constant with η as is shown in Fig. 1.3. The E_t distributions are steeply falling, as is shown in Fig. 1.4. The mean E_t for these distributions is 223 MeV for

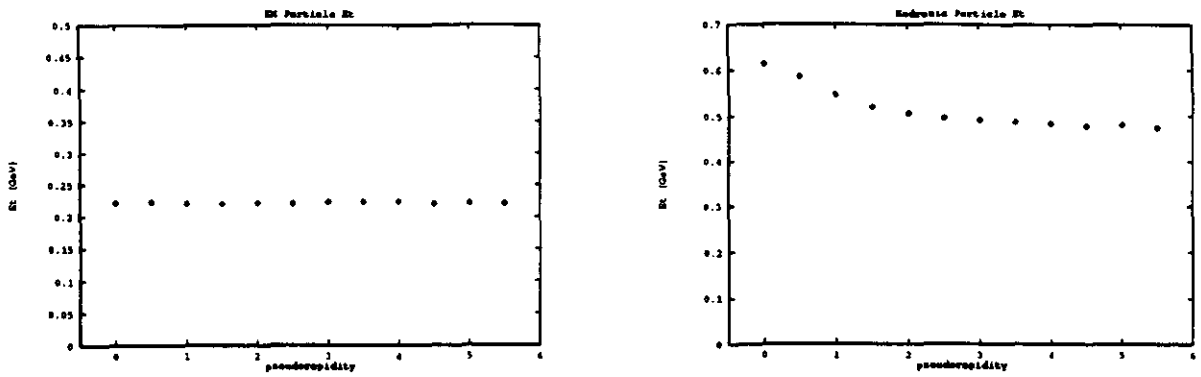

Figure 1.2: The electromagnetic (left) and hadronic (right) E_t/particle as a function of η in jets produced by ISAJET.

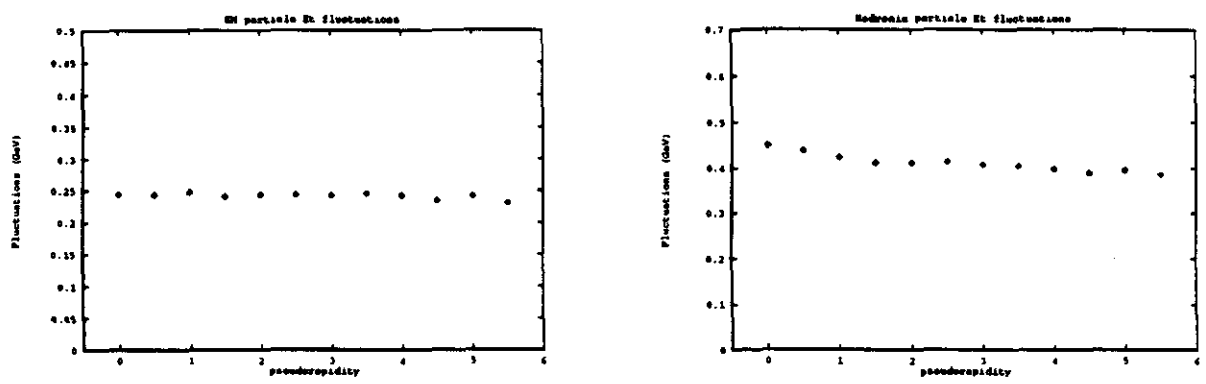

Figure 1.3: The fluctuations on particle E_t as produced by ISAJET as a function of η.

electromagnetic, and 512 MeV for hadronic, with a width (second moment around mean) of 244 MeV (EM) and 416 MeV (HAD).

Events were generated using the above specifications. For instance, an average of 9 electromagnetic particles are produced per rapidity interval so on average, 54 electromagnetic particles are produced uniformly distributed between η of 0 and 6. The actual number produced is drawn from a Poisson distribution. The particles are produced with a transverse energy drawn from the appropriate distribution in Fig. 1.4. Then the actual energy is calculated by dividing by $\sin\theta$. We generated 100000 events in this way.

The model of energy deposition in the calorimeter is very simple. A particle deposits energy in a calorimeter cell if its shower circle overlaps the center of the cell. The amount of energy deposited is the energy of the particle multiplied by the ratio of the cell area to the shower area (areas in cm^2). This ignores the non-uniform profile of showers, and partial illumination of the cell by the shower, but for small cells and large showers, it is

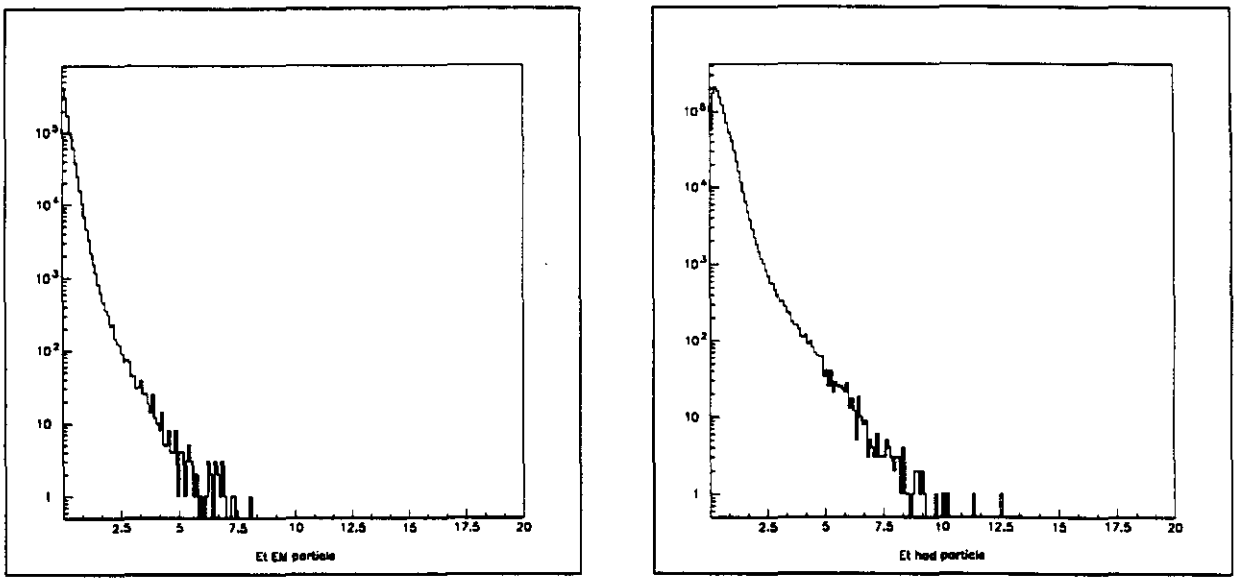

Figure 1.4: The E_t per particle in ISAJET produced two jet pileup events for electromagnetic (left) and hadronic (right) particles.

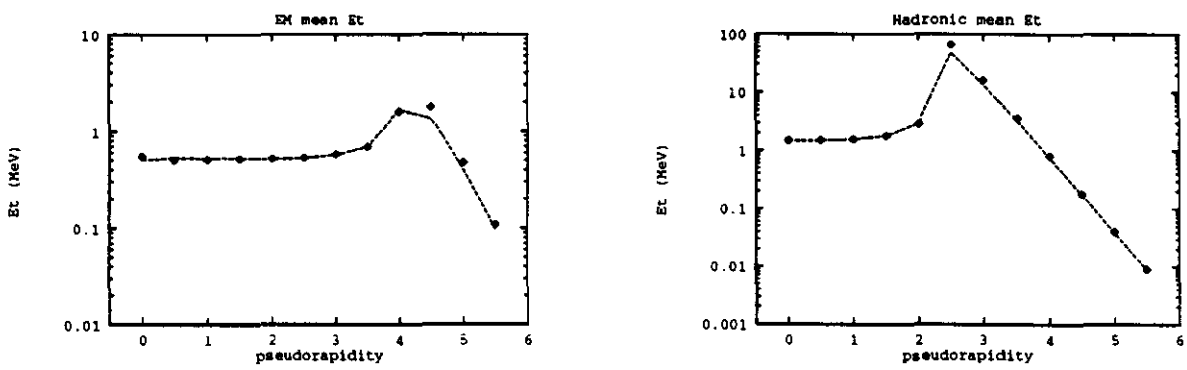

Figure 1.5: The mean E_t deposited in a simulated calorimeter cell from electromagnetic particles (left) and hadronic particles (right) as a function of η. The points are the result of the Monte Carlo simulation, while the curve is the analytic model.

a reasonable approximation. Since an electromagnetic shower in this model has a radius of 2.2 cm and the cell at $\eta = 2.5$ is about half a centimeter on a side, this regime applies.

Twelve cells distributed at half unit intervals in pseudorapidity from 0.0 to 5.5 were monitored and the mean and variance of their energy deposits accumulated. The result as a function of η is shown as the points in Fig. 1.5 and Fig. 1.6 for both the electromagnetic and hadronic sections.

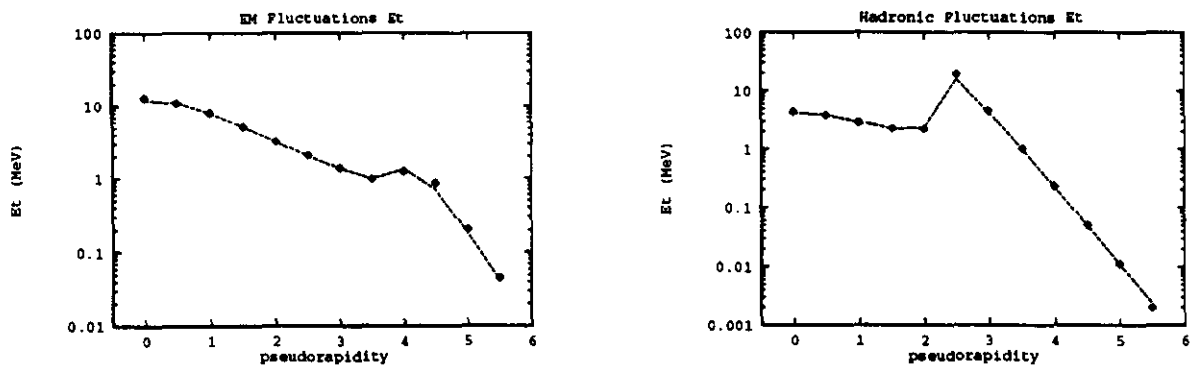

Figure 1.6: The fluctuations of deposited E_t in a simulated calorimeter cell from electromagnetic (left) and hadronic (right) particles. The points are the result of the Monte Carlo simulation while the curve is the analytic model.

We see that the trend is for a decreasing mean E_t for both electromagnetic and hadronic depositions, however there is a dramatic jump in the distribution at $\eta = 4$ for electromagnetic and $\eta = 2.5$ for hadronic energy. We next build an analytic description of the system and understand this behavior.

2. Analytic Model

The transverse energy signal in a cell will be given by given by

$$E_t = \sum_i^N E_i \times \sin\theta_{\text{cell}} \frac{\text{cell area}}{\text{shower area}} \tag{2.1}$$

A random number N of particles will have showers that overlap the cell. The energy E_i of particle i is $E_{t_i}/\sin\theta_i$. It is useful to recast Eq. (2.1) in terms of E_t since the transverse energy distribution is universal, so:

$$\begin{aligned} E_t &= \sum_i^N \frac{E_{t_i}}{\sin\theta_i} \times \sin\theta_{\text{cell}} \frac{\text{cell area}}{\text{shower area}} \\ &= \sum_i^N \frac{E_{t_i}}{\cosh\eta_{\text{cell}}} \times \cosh\eta_i \frac{\text{cell area}}{\text{shower area}} \end{aligned} \tag{2.2}$$

since $\sin\theta_i$ equals $1/\cosh\eta_i$.

The number N in Eq. (2.2) is the number of particles with showers that overlap the cell in consideration. This is the number of particles that strike the calorimeter within a

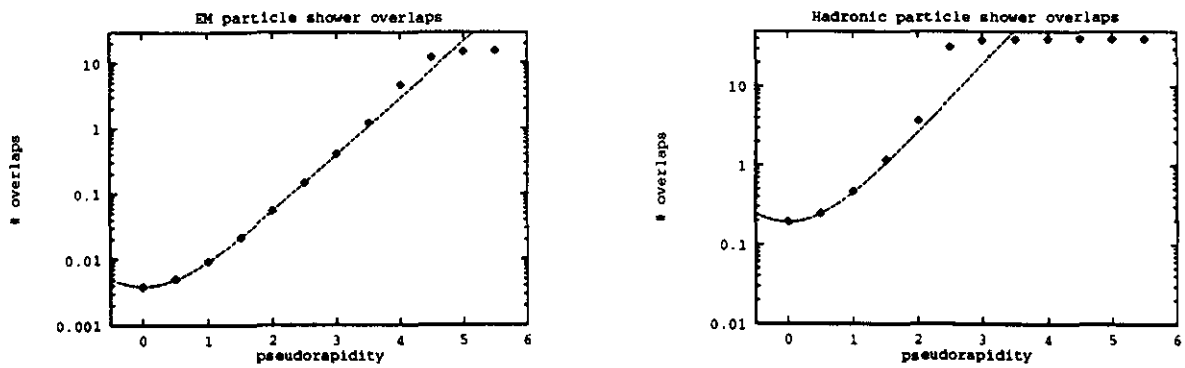

Figure 2.1: The average number of particles whose showers overlap a point at the given η. Electromagnetic particles have smaller showers than hadronic particles, giving fewer overlaps. A plot of $a\cosh^2\eta$ is overlaid with the appropriate value of a.

circle whose radius is given by the shower size. This number is

$$\begin{aligned} N_{EM} &= \rho_{EM}\frac{\pi r_{EM}^2}{R_c^2}\cosh^2\eta \\ N_{HAD} &= \rho_{HAD}\frac{\pi r_{HAD}^2}{R_c^2}\cosh^2\eta \end{aligned} \tag{2.3}$$

where ρ_{EM} and ρ_{HAD} are the electromagnetic and hadronic particle densities $d^2N/d\eta d\phi$, r_{EM} and r_{HAD} are the electromagnetic nad hadronic shower radii, and R_c is the radius of the calorimeter.

The hyperbolic cosine comes from the conversion from $d^2N/d\eta d\phi$ to $dN/d\Omega$. Note that the hyperbolic cosine is a rapidly (exponentially) increasing function of its argument.

Equation (2.2) includes a factor for the ratio between the cell area and the shower area. A cell specified by $\Delta\eta\Delta\phi$ has an area of $R_c^2\Delta\eta\Delta\phi\,\mathrm{sech}^2\eta$. A segmentation of $\Delta\eta\Delta\phi = 0.04\times 0.04$ in a calorimeter at radius 75 cm gives cells with area $9.00\,\mathrm{sech}^2\eta\,\mathrm{cm}^2$.

The shower area is determined just by the physical parameters of the detector, and is different for electromagnetic and hadronic particles. Since we have assumed radii of 2.2 cm and 14.0 cm for electromagnetic and hadronic showers, their areas are 15.20 and 615.75 cm^2. The hyperbolic secant has an exponential decay with increasing η so the cell size to shower size ratio in Eq. (2.2) is decreasing with η.

2.1. Shower overlaps

From the simulation, we can directly determine the number of particles per event that overlap each sampling point and compare it it to the prediction of Eq. (2.3). Knowing that there are 9 electromagnetic particles and 11 hadronic particles per unit of rapidity

determines that $\rho_{EM} = 1.432$ and $\rho_{HAD} = 1.751$. These along with the values of the shower size and calorimeter radius, predict that:

$$\begin{aligned} N_{EM} &= 0.0039 \cosh^2 \eta \\ N_{HAD} &= 0.191 \cosh^2 \eta \end{aligned} \tag{2.4}$$

The number of overlaps per simulated event occuring at each sampling point is plotted in Fig. 2.1 along with the prediction of Eq. (2.4). At low η, the mean number of overlaps follow the prediction quite well, especially for the electromagnetic case, but at high η the Monte Carlo shows a deviation from the simple model. The model predicts ever increasing numbers of particles as η increases, but this is clearly unphysical past a certain point. A real calorimeter will only have coverage out to a maximum η of 5.5–6. At some point maximal overlap occurs such that all the available particles overlap an extended region in η. We can calculate the point at which this occurs.

A calorimeter with coverage out to $\eta = 6$ goes down to angles of 4.96 mrad. An electromagnetic shower with a width of 2.2 cm in a calorimeter that has a 75 cm radius has a width in θ of 29.33 mrad. So, an electromagnetic particle that showers at $\eta = 4$ corresponding to $\theta = 36.63$ mrad will not overlap the edge of the calorimeter at $\eta = 6$, while a particle showering at $\eta = 4.5$ will. This results in the behavior seen in Fig. 2.1 where the EM overlaps become constant after $\eta = 4.5$. A similar calculation for the wider hadronic showers show that after a pseudorapidity of about 2.5, showers are overlapping the edge of the calorimeter.

Not coincidentally, this is also the place where the mean E_t takes such an abrupt jump. Consider what happens to a cell at $\eta = 4.5$ when an electromagnetic particle with $E_t = 223$ MeV strikes the calorimeter at $\eta = 5.9$. The shower produced by this particle has a radius of 2.2 cm corresponding to an angle of 29.3 mrad. This shower overlaps the cell at $\eta = 4.5$. Energy that this cell measures is weighted by the value of $\sin\theta$ appropriate at $\eta = 4.5$. However, the particle that produced the energy deposit had a transverse energy of 223 MeV at $\eta = 5.9$ which means it had an actual energy of 40 GeV. So we see that at this point, particles are contributing energy to measurement of transverse energy with a weight which is much larger than it should be.

The mean number of showers overlapping a sampling point will be needed later in the calculation, so we tabulate the number of overlaps according to the simulation in Table 2.1.

2.2. Mean E_t

Due to the finite shower size, a particular cell will sample particles striking the detector over a range of pseudorapidities. The physical size of the range depends on whether the shower is electromagnetic or hadronic, but because cells that have a constant size in $\Delta\eta\Delta\phi$ decrease in size with increasing pseudorapidity, the space that the shower occupies increases in $\eta\phi$ space. We tabulate the ranges contribute to each of the sampling points for electromagnetic and hadronic showers in Table 2.2.

To find the measured mean E_t, we just take the expectation value of Eq. (2.2).

$$\langle E_t \rangle = \frac{\text{cell area}}{\text{shower area}} \frac{1}{\cosh \eta_{\text{cell}}} \left\langle \sum_i^N E_{t_i} \cosh \eta_i \right\rangle \tag{2.5a}$$

Table 2.1: The mean number of overlaps at each sampled point in η as determined by the event simulation. Hadronic showers have more overlaps than electromagnetic showers at any η point because of their larger shower radius.

η	N_{EM}	N_{HAD}
0.0	0.0038	0.1927
0.5	0.0051	0.2478
1.0	0.0094	0.4715
1.5	0.0214	1.164
2.0	0.0549	3.683
2.5	0.1475	31.91
3.0	0.4109	38.15
3.5	1.211	39.38
4.0	4.612	39.77
4.5	12.173	39.91
5.0	14.945	39.96
5.5	15.650	39.98

Table 2.2: The pseudorapidity range that contributes energy to each of the sampled points for both electromagnetic and hadronic showers.

η	Electromagnetic		Hadronic	
	η_l	η_h	η_l	η_h
0.0	-0.03	0.03	-0.19	0.19
0.5	0.47	0.53	0.30	0.72
1.0	0.95	1.05	0.74	1.33
1.5	1.43	1.57	1.13	2.06
2.0	1.90	2.12	1.46	3.19
2.5	1.22	2.70	1.73	6.00
3.0	2.74	3.35	1.94	6.00
3.5	3.10	4.16	2.09	6.00
4.0	3.41	5.61	2.19	6.00
4.5	3.66	6.00	2.26	6.00
5.0	3.84	6.00	2.30	6.00
5.5	3.98	6.00	2.32	6.00

$$= F \operatorname{sech}^2 \eta_{\text{cell}} \frac{\langle N \rangle}{\cosh \eta_{\text{cell}}} \langle E_{t_i} \cosh \eta_i \rangle \tag{2.5b}$$

$$= F\,\mathrm{sech}^2\,\eta_{\mathrm{cell}}\,\langle N\rangle \frac{\langle E_t\rangle}{\cosh\eta_{\mathrm{cell}}}\frac{1}{\eta_h-\eta_l}\int_{\eta_l}^{\eta_h}\cosh\eta\,d\eta \tag{2.5c}$$

$$= F\,\mathrm{sech}^2\,\eta_{\mathrm{cell}}\,\langle N\rangle\langle E_t\rangle J(\eta_{\mathrm{cell}}) \tag{2.5d}$$

where

$$\begin{aligned} J(\eta) &= \frac{1}{\cosh\eta}\,\frac{1}{\eta_h-\eta_l}\int_{\eta_l}^{\eta_h}\cosh\eta\,d\eta \\ &= \frac{1}{\cosh\eta}\,\frac{\sinh\eta_h-\sinh\eta_l}{\eta_h-\eta_l} \end{aligned} \tag{2.6}$$

In formula (2.5c), F is the constant term in the ratio of the cell area to the shower area and has the value $0.592 = 9.0/15.2$ for electromagnetic showers, and $0.0147 = 9.0/615.75$ for hadronic showers. Use has been made of the result of Eq. (I.4) to replace the sum over N of the individual $E_t\cosh\eta$ with the product of $\langle N\rangle\langle E_t\rangle\cosh\eta$ which results in the integral. The value of $\langle N\rangle$ is the mean number of overlaps from Table 2.1 while the value of $\langle E_t\rangle$ is either 223 MeV or 512 MeV, the mean of the appropriate distribution in Fig. 1.4. The limits on the integral η_l,η_h are the pseudorapidity ranges which contribute to a cell that were tabulated in Table 2.2. The integral over $d\eta$ is appropriate because the particle density is constant in η space.

We see that different terms in the final result Eq. (2.5c) vary differently with pseudorapidity. First of all, the term $\mathrm{sech}^2\,\eta$ which is for the ratio of the cell area to the shower area is rapidly decreasing with η. In fact, in this region, the hyperbolic secant becomes approximately an exponential. The exponential character of the decrease is evident in Fig. 1.5 in the last several points of the graph. The number of overlaps $\langle N\rangle$ starts by increasing with η and becomes constant. The factor J, involving the difference of hyperbolic sines over the hyperbolic cosine can be thought of as a correction factor accounting for the nonzero width of the shower. This factor is unity near 90° and becomes large at the point where the number of overlaps becomes constant, and then decreases again because the difference $\eta_h-\eta_l$ becomes smaller. This is the factor responsible for the sudden jump in the mean E_t.

3. E_t Fluctuations

We now calculate the fluctuations on E_t. From Eq. (I.6) and Eq. (2.2),

$$\mathrm{Var}\,(E_t) = \mathrm{Var}\left(\frac{\text{cell area}}{\text{shower area}}\,\frac{1}{\cosh\eta_{\mathrm{cell}}}\sum_i^N E_{t_i}\cosh\eta_i\right) \tag{3.1a}$$

$$= \left[F\,\mathrm{sech}^2\,\eta_{\mathrm{cell}}\right]^2\ \mathrm{Var}\left(\frac{1}{\cosh\eta_{\mathrm{cell}}}\sum_i^N E_{t_i}\cosh\eta_i\right) \tag{3.1b}$$

$$= \left[F\,\mathrm{sech}^2\,\eta_{\mathrm{cell}}\right]^2\left\{\frac{\langle N\rangle}{\cosh^2\eta_{\mathrm{cell}}}\mathrm{Var}\,(E_t\cosh\eta) + \frac{\mathrm{Var}\,(N)}{\cosh^2\eta_{\mathrm{cell}}}\langle E_t\cosh\eta\rangle^2\right\} \tag{3.1c}$$

$$= \left[F\,\mathrm{sech}^2\,\eta\right]^2\left\{\frac{\langle N\rangle}{\cosh^2\eta_{\mathrm{cell}}}\mathrm{Var}\,(E_t\cosh\eta) + \mathrm{Var}\,(N)\,\langle E_t\rangle^2 J^2(\eta)\right\} \tag{3.1d}$$

using the same definitions as in Eq. (2.5). $\mathrm{Var}(N)$ is the contribution to E_t fluctuations coming from the fluctuations in the number of overlaps. In this simulation, the number of overlaps follows Poisson statistics so that $\mathrm{Var}(N) = \langle N \rangle$ but in the general case this will not be the case. Poisson counting assumes that each count is independent of the others, but the particles in a region of an event are correlated since particles are generally produced in jets.

Evaluating $\mathrm{Var}(E_t \cosh \eta)$:

$$\begin{aligned}
\frac{1}{\cosh \eta_{\mathrm{cell}}^2} \mathrm{Var}\left(E_t \cosh \eta\right) &= \frac{1}{\cosh^2 \eta_{\mathrm{cell}}} \left(\langle E_t^2 \cosh^2 \eta \rangle - \langle E_t \cosh \eta \rangle^2\right) \\
&= \frac{\langle E_t^2 \rangle}{\cosh^2 \eta_{\mathrm{cell}}} \frac{1}{\eta_h - \eta_l} \int_{\eta_l}^{\eta_h} \cosh^2 \eta \, d\eta \quad - \quad \langle E_t \rangle^2 J^2(\eta) \\
&= \langle E_t^2 \rangle H(\eta) - \langle E_t \rangle^2 J^2(\eta)
\end{aligned} \tag{3.2}$$

where $H(\eta)$ is the value of the integral:

$$\begin{aligned}
H(\eta) &= \frac{1}{\cosh^2 \eta_{\mathrm{cell}}} \frac{1}{\eta_h - \eta_l} \int_{\eta_l}^{\eta_h} \cosh^2 \eta \, d\eta \\
&= \frac{1}{\cosh^2 \eta_{\mathrm{cell}}} \left[\frac{1}{2} + \frac{1}{4} \frac{\sinh 2\eta_h - \sinh 2\eta_l}{\eta_h - \eta_l}\right]
\end{aligned} \tag{3.3}$$

With these definitions of J and H and combining with equations (3.1) and (3.2) we can write:

$$\begin{aligned}
\mathrm{Var}\left(E_t\right) = \left[F \operatorname{sech}^2 \eta_{\mathrm{cell}}\right]^2 \; &\left[\langle N \rangle \langle E_t^2 \rangle H(\eta_{\mathrm{cell}})\right. \\
&\left. + \left(\mathrm{Var}\left(N\right) - \langle N \rangle\right) \langle E_t \rangle^2 J^2(\eta_{\mathrm{cell}})\right]
\end{aligned} \tag{3.4}$$

The numerical values of J and H are listed in Table 3.1. Since they depend on the pseudorapidity range for each sampled point which depends on the shower size, there are different values for J and H for electromagnetic and hadronic showers.

The final analytic results for $\langle E_t \rangle$ and $\sigma_{E_t} = \sqrt{\mathrm{Var}(E_t)}$ are listed in Table 3.2 and Table 3.3 along with their values from the simulation. This shown graphically in Fig. 1.5 and Fig. 1.6.

As can be seen from the tables and figures, the agreement between the analytic model and the simulation is very good, giving us confidence that we understand the origin of the pseudorapidity behavior of the mean and fluctuations of E_t depositions in a calorimeter of this type. While a physical calorimeter will certainly be different in many respects, to the extent that it has the same features is this simulated calorimeter these effects will be manifest.

Table 3.1: The values of the functions J and H for both electromagnetic and hadronic cells used in calculating the mean and variance of E_t in the analytic model.

η	Electromagnetic		Hadronic	
	J	H	J	H
0.0	1.000	1.000	1.006	1.012
0.5	1.000	1.001	1.012	1.028
1.0	1.001	1.002	1.040	1.101
1.5	1.003	1.007	1.132	1.361
2.0	1.008	1.019	1.550	2.951
2.5	1.022	1.055	7.601	126.726
3.0	1.062	1.163	4.849	49.398
3.5	1.198	1.568	3.049	18.920
4.0	2.028	5.653	1.896	7.154
4.5	1.730	4.248	1.169	2.680
5.0	1.115	1.690	0.716	0.998
5.5	0.707	0.660	0.437	0.370

Table 3.2: The mean E_t deposition calculated analytically and by simulation shown for electromagnetic and hadronic cells. These are the data that are plotted in Fig. 1.5.

η	Electromagnetic		Hadronic	
	Analytic	Simulated	Analytic	Simulated
0.0	0.502	0.552	1.451	1.475
0.5	0.530	0.500	1.477	1.493
1.0	0.522	0.511	1.543	1.546
1.5	0.512	0.507	1.784	1.779
2.0	0.516	0.519	3.020	2.965
2.5	0.529	0.530	48.298	66.273
3.0	0.568	0.576	13.666	15.859
3.5	0.697	0.692	3.273	3.575
4.0	1.655	1.593	0.757	0.800
4.5	1.372	1.772	0.172	0.179
5.0	0.399	0.472	0.039	0.040
5.5	0.098	0.108	0.009	0.009

Table 3.3: The fluctuations of E_t depositions ($\sqrt{\mathrm{Var}(E_t)}$ calculated analytically and by simulation shown for electromagnetic and hadronic cells. These data are plotted in Fig. 1.6.

η	Electromagnetic		Hadronic	
	Analytic	Simulated	Analytic	Simulated
0.0	12.073	12.954	4.260	4.332
0.5	11.002	10.966	3.831	3.850
1.0	7.982	8.013	2.920	2.916
1.5	5.194	5.198	2.195	2.185
2.0	3.273	3.303	2.247	2.162
2.5	2.054	2.093	16.316	19.763
3.0	1.336	1.346	4.132	4.494
3.5	0.982	0.971	0.959	1.008
4.0	1.341	1.248	0.218	0.225
4.5	0.695	0.853	0.049	0.050
5.0	0.179	0.202	0.011	0.011
5.5	0.042	0.045	0.002	0.002

I. Sum of a random number of random variables

Suppose a random variable Y is made from the sum of a random number n of independent and identically distributed random variables X. What is the mean and variance of Y?

$$Y = \sum_{i=1}^{n} X_i \tag{I.1}$$

Denote Y_n as the sum of n instances of the variable X:

$$Y_n = \sum_{i=1}^{n} X_i \tag{I.2}$$

We know the mean and variance of Y_n from the mean and variance of X:

$$\begin{aligned} \langle Y_n \rangle &= n\langle X \rangle \\ \mathrm{Var}\,(Y_n) &= n\mathrm{Var}\,(X) \end{aligned} \tag{I.3}$$

We are now in a position to calculate the moments of Y. Let $\mathrm{P}(n)$ be the probability that Y is the sum of n instances of X. Then

$$\begin{aligned} \langle Y \rangle &= \sum_n \mathrm{P}\,(n)\,\langle Y_n \rangle \\ &= \sum_n \mathrm{P}\,(n)\,n\langle X \rangle \\ &= \bar{n}\langle X \rangle \end{aligned} \tag{I.4}$$

The variance of Y is $\langle Y^2\rangle - \langle Y\rangle^2$. We know what $\langle Y\rangle^2$ is; we now calculate $\langle Y^2\rangle$:

$$\langle Y^2\rangle = \sum_n \mathrm{P}(n)\,\langle Y_n^2\rangle \tag{I.5}$$

but

$$\begin{aligned}\langle Y_n^2\rangle &= \mathrm{Var}(Y_n) + \langle Y_n\rangle^2 \\ &= n\mathrm{Var}(X) + n^2\langle X\rangle^2\end{aligned}$$

Putting this in Eq. (I.5) gives

$$\begin{aligned}\mathrm{Var}\left(Y^2\right) &= \sum_n \mathrm{P}(n)\left[n\mathrm{Var}(X) + n^2\langle X\rangle^2\right] \\ &= \bar{n}\mathrm{Var}(X) + \bar{n^2}\langle X\rangle^2\end{aligned}$$

Resulting in

$$\begin{aligned}\mathrm{Var}(Y) &= \bar{n}\mathrm{Var}(X) + \bar{n^2}\langle X\rangle^2 - \bar{n}^2\langle X\rangle^2 \\ &= \bar{n}\mathrm{Var}(X) + \left[\bar{n^2} - \bar{n}^2\right]\langle X\rangle^2 \\ &= \bar{n}\mathrm{Var}(X) + \mathrm{Var}(n)\,\langle X\rangle^2\end{aligned} \tag{I.6}$$

References

1. W. E. Cleland *et al.*, "Pileup and Thermal Noise in a Liquid Ionization Calorimeter", in *Proceedings of the Symposium on Detector Research and Development for the Superconducting Super Collider*, Oct. 15–18 1990, Fort Worth, TX, World Scientific Publishing Co., Singapore..
2. W. E. Cleland, E. G. Stern, SSC Ionization Calorimeter Studies, *in preparation.*
3. F. E. Paige and S. D. Protopopescu in *Snowmass Summer Study 1996*, S. Donaldson and J. Marx, eds..